INTERNATIONAL JOURNAL FOR NUMERICAL METHODS IN ENGINEERING
Int. J. Numer. Meth. Engng 2007; **72**:697–721
Published online 28 March 2007 in Wiley InterScience (www.interscience.wiley.com). DOI: 10.1002/nme.2031

An incremental formulation for the prediction of two-dimensional fatigue crack growth with curved paths

Ki-Seok Kim[1,‡] and Hae Sung Lee[2,*,†,§]

[1]*Steel Structure Research Laboratory, Research Institute of Industrial Science & Technology, Korea*
[2]*Department of Civil, Urban and Geosystem Engineering, Seoul National University, Korea*

SUMMARY

This paper presents a new incremental formulation for predicting the curved growth paths of two-dimensional fatigue cracks. The displacement and traction boundary integral equations (BIEs) are employed to calculate responses of a linear elastic cracked body. The Paris law and the principle of local symmetry are adopted for defining the growth rate and direction of a fatigue crack, respectively. The three governing equations, i.e. the BIEs, the Paris law and the local symmetry condition, are non-linear with respect to the crack growth path and unknowns on the boundary. Iterative forms of three governing equations are derived to solve problems of the fatigue crack growth by the Newton–Raphson method. The incremental crack path is modelled as a parabola defined by the crack-tip position, and the trapezoidal rule is employed to integrate the Paris law. The validity of the proposed method is demonstrated by two numerical examples of plates with an edge crack. Copyright © 2007 John Wiley & Sons, Ltd.

Received 26 December 2005; Revised 30 January 2007; Accepted 5 February 2007

KEY WORDS: fatigue crack growth; boundary integral equation; Paris law; principle of local symmetry; Newton–Raphson method

1. INTRODUCTION

The phenomenon of fatigue is of great importance in designs of steel structures. Numerous experiments and researches based on linear elastic fracture mechanics have been performed for the prediction of fatigue crack growth [1, 2]. A fatigue crack usually does not grow straight due to mixed-mode loads or asymmetric geometry [3]. The prediction of the growth path and evaluation

*Correspondence to: Hae Sung Lee, Department of Civil, Urban and Geosystem Engineering, Seoul National University, San 56-1, Shillim-dong, Kwanak-gu, Seoul 151-742, Korea.
†E-mail: chslee@snu.ac.kr
‡Senior Researcher.
§Professor.

Contract/grant sponsor: Korea Ministry of Construction & Transportation

of the fatigue life have been major issues in the analysis of fatigue crack growth. The fatigue life is the number of load cycles required to have the crack grow to the critical length, at which the equivalent stress intensity factor (SIF) reaches the fracture toughness of a material.

The growth path of a fatigue crack and other physical quantities are determined for a given loading history by solving three governing equations simultaneously; the governing equation of an elastic cracked body, the Paris law for the crack growth rate, and the criterion of growth direction. Since the three governing equations of fatigue crack growth form a coupled non-linear system with respect to the unknown growth path and responses of the cracked body, an incremental approach is widely adopted. In the incremental approach, the total load cycles are divided into small increments of load cycles, and the governing equations are solved for each increment sequentially. The efficiency of a solution method is represented by the largest size of an increment that can achieve the required accuracy of solutions.

The tangent approach, in which the growth rate and direction of a crack is determined based on the current crack configuration without iterative corrections [4–9], is widely employed in the analyses of fatigue crack growth due to its simplicity. Since, however, the growth direction and rate change continuously during an increment of load cycles, the tangent approach generally yields inaccurate crack paths, and overestimates the fatigue life unless increments of load cycles are kept small.

A few iterative schemes have been proposed to predict a curved crack path for a predefined incremental crack length [10–13]. However, the fatigue crack growth should be analysed for a predefined load cycle rather than a predefined crack length, and thus previously proposed iterative schemes are not directly applicable to fatigue crack growth. Moreover, since the Paris law defining the growth rate is a non-linear implicit function of a crack path, the incremental crack length should be iteratively corrected along with the growth direction of a fatigue crack simultaneously. Another shortcoming of the previous iterative schemes is that the crack-tip position is not included as unknown in the system equations of fatigue crack growth, but is assumed for the analysis of a cracked body. The assumed crack-tip position is updated iteratively based on results of the analysis, which causes slow convergence and requires a rather small increment of load cycles.

This paper presents a new incremental formulation to overcome the shortcomings of the previous approaches. In the proposed method, the three governing equations of the fatigue crack growth are solved simultaneously for boundary unknowns and crack-tip position for predicting the growth path of a fatigue crack for a given increment of load cycles. The displacement and traction boundary integral equations (BIEs) [6–8, 10, 14, 15] are employed to analyse a linear elastic body with a crack, and are discretized by the boundary element method (BEM) [16, 17]. The crack growth is simulated by adding a new boundary element along the crack extension. The singularity of stress field near the crack tip is taken into account using the singular element proposed by Kebir *et al*. [7]. The Paris law [1, 2, 18] and the principle of local symmetry (PLS) [11, 12, 19] are adopted to define the growth path. The incremental crack length is obtained by integrating the Paris law for a given increment of load cycles, and the incremental crack path is modelled as a parabolic curve represented by the unknown crack-tip position. Since the crack-tip position for a given increment of load cycles is unknown, the discretized BIEs include the crack-tip position as unknowns. The mixed-mode SIFs are evaluated by the displacement extrapolation method using the crack opening displacement (COD) [7]. The three discretized governing equations are linearized and solved by the Newton–Raphson method for the unknowns on the boundary and the crack-tip position.

DOI: 10.1002/nme

Two numerical examples are presented to demonstrate the validity of the proposed method. In the first example, a fatigue crack grows along an almost straight path from an inclined initial edge crack in a plate under a tensile load. An edge crack of a plate under mode II loading condition, which exhibits a curved growth path, is presented in the second example. It is shown that the proposed method gives more accurate and stable results than the tangent approach for a larger increment of load cycles.

2. GOVERNING EQUATIONS OF FATIGUE CRACK GROWTH

This chapter presents governing equations of fatigue crack growth. The displacement BIE is applied on the exterior boundary of the body, while the traction BIE is used on the traction-free crack surface. The Paris law is adopted to define the growth rate of a fatigue crack. The growth direction of a crack is determined by the PLS.

2.1. Displacement and traction BIEs

Figure 1 shows the geometry and boundary conditions of a cracked body subject to fatigue loads. Either displacement $\mathbf{u}$ or traction $\mathbf{q}$ is prescribed on the exterior boundary of the cracked body, Γ.

$$\mathbf{u} = \overline{\mathbf{u}} \quad \text{on } \Gamma_u \tag{1a}$$

$$\mathbf{q} = \overline{\mathbf{q}} \quad \text{on } \Gamma_q \tag{1b}$$

where $\Gamma_u \cup \Gamma_q = \Gamma$, $\Gamma_u \cap \Gamma_q = \emptyset$, and $\overline{\mathbf{u}}$ and $\overline{\mathbf{q}}$ are the prescribed displacement and traction, respectively. It is assumed that a proportional cyclic fatigue load with a constant amplitude is applied on Γ_q, and that no traction is applied on the crack surface Γ_c where $\Gamma_c \cap \Gamma_u = \emptyset$ and $\Gamma_c \cap \Gamma_q = \emptyset$. The crack path, $\boldsymbol{\chi}$, is represented by the parametric form of a curve.

$$\boldsymbol{\chi}(\tau) = (\chi_1(\tau), \chi_2(\tau)) \quad (0 \leqslant \tau \leqslant \overline{\tau}) \tag{2}$$

where τ is a curve parameter and $\overline{\tau}$ is the prescribed curve parameter at the crack tip.

The displacement and traction BIEs [6–8, 10, 14, 15] are employed to calculate responses of the linear elastic body with a crack. The displacement BIE on the exterior boundary and the traction BIE on crack surface are obtained by applying the reciprocal theorem between the real solution and

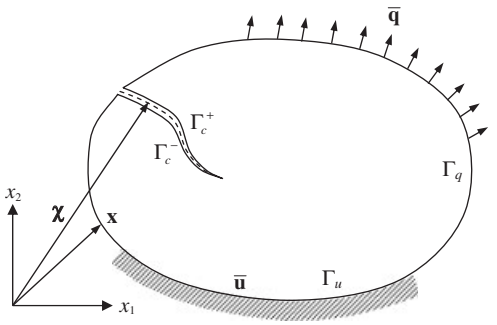

Figure 1. Geometry and boundary conditions of a cracked elastic body.

DOI: 10.1002/nme

the fundamental solution as follows [6]:

$$\mathbf{B}_u(\boldsymbol{\xi}, \mathbf{x}) \equiv \mathbf{c}(\boldsymbol{\xi})\mathbf{u}_s(\boldsymbol{\xi}) + \oint_{\Gamma_q} \mathbf{T}(\boldsymbol{\xi}, \mathbf{x})\mathbf{u}(\mathbf{x})\,\mathrm{d}\Gamma + \int_{\Gamma_c} \mathbf{T}(\boldsymbol{\xi}, \boldsymbol{\chi})\mathbf{u}(\boldsymbol{\chi})\,\mathrm{d}\Gamma - \int_{\Gamma_u} \mathbf{S}(\boldsymbol{\xi}, \mathbf{x})\mathbf{q}(\mathbf{x})\,\mathrm{d}\Gamma - \int_{\Gamma_q} \mathbf{S}(\boldsymbol{\xi}, \mathbf{x})\overline{\mathbf{q}}(\mathbf{x})\,\mathrm{d}\Gamma = \mathbf{0} \quad \text{for } \boldsymbol{\xi} \in \Gamma \tag{3}$$

$$\mathbf{B}_q(\boldsymbol{\xi}, \mathbf{x}) \equiv \mathbf{n}_s(\boldsymbol{\xi}) \cdot \left(\int_{\Gamma_q} \mathbf{T}^{\sigma}(\boldsymbol{\xi}, \mathbf{x})\mathbf{u}(\mathbf{x})\,\mathrm{d}\Gamma + \oint\!\!\!\!\!\!= \int_{\Gamma_c} \mathbf{T}^{\sigma}(\boldsymbol{\xi}, \boldsymbol{\chi})\mathbf{u}(\boldsymbol{\chi})\,\mathrm{d}\Gamma - \int_{\Gamma_u} \mathbf{S}^{\sigma}(\boldsymbol{\xi}, \mathbf{x})\mathbf{q}(\mathbf{x})\,\mathrm{d}\Gamma - \int_{\Gamma_q} \mathbf{S}^{\sigma}(\boldsymbol{\xi}, \mathbf{x})\overline{\mathbf{q}}(\mathbf{x})\,\mathrm{d}\Gamma \right) = \mathbf{0} \quad \text{for } \boldsymbol{\xi} \in \Gamma_c \tag{4}$$

where $\boldsymbol{\xi}$, $\mathbf{x}$, $\mathbf{c}$, $\mathbf{u}_s$, and $\mathbf{n}_s$ denote the co-ordinates of a source point and a field point on the boundary, jump term, displacement and outward normal vector at a source point, respectively. $\mathbf{S}$ and $\mathbf{T}$ are the displacement and traction kernels for the displacement BIE of a two-dimensional body, respectively. The kernels for the traction BIE, $\mathbf{S}^{\sigma}$ and $\mathbf{T}^{\sigma}$, are linear combinations of the derivatives of $\mathbf{S}$ and $\mathbf{T}$ with respect to a source point, respectively [16, 17]. Refer to Appendix A.1 for the detailed expressions of the kernels. The integral symbols, $\oint$ and $\oint\!\!\!\!\!\!=$, imply the Cauchy and the Hadamard principal-value integral, respectively. In the derivation of (3) and (4), it is assumed that the prescribed displacement on Γ_u is zero.

Since the traction kernels on the opposite surfaces of a crack have the same magnitudes with different signs, the boundary integral terms on the crack surface are expressed as single-path integrals in terms of the COD.

$$\int_{\Gamma_c} \mathbf{T}(\boldsymbol{\xi}, \boldsymbol{\chi})\mathbf{u}(\boldsymbol{\chi})\,\mathrm{d}\Gamma = \int_0^{\overline{\tau}} \mathbf{T}(\boldsymbol{\xi}, \boldsymbol{\chi})\mathbf{u}^c(\boldsymbol{\chi})J(\boldsymbol{\chi})\,\mathrm{d}\tau \tag{5a}$$

$$\oint\!\!\!\!\!\!= \int_{\Gamma_c} \mathbf{T}^{\sigma}(\boldsymbol{\xi}, \boldsymbol{\chi})\mathbf{u}(\boldsymbol{\chi})\,\mathrm{d}\Gamma = \oint\!\!\!\!\!\!= \int_0^{\overline{\tau}} \mathbf{T}^{\sigma}(\boldsymbol{\xi}, \boldsymbol{\chi})\mathbf{u}^c(\boldsymbol{\chi})J(\boldsymbol{\chi})\,\mathrm{d}\tau \tag{5b}$$

where $\mathbf{u}^c$ is the COD, which is defined as $\mathbf{u}^c = \mathbf{u}^+ - \mathbf{u}^-$. Here, the signs $(+)$ and $(-)$ indicate the opposite surfaces of a crack, respectively, and J is the Jacobian of the crack surface with respect to the curve parameter.

$$J(\boldsymbol{\chi}(\tau)) = \|\boldsymbol{\chi}'(\tau)\|_2 = \sqrt{\left(\frac{\mathrm{d}\chi_1}{\mathrm{d}\tau}\right)^2 + \left(\frac{\mathrm{d}\chi_2}{\mathrm{d}\tau}\right)^2} \tag{6}$$

where $(\,)'$ and $\|\,\|_2$ represent the differentiation with respect to the curve parameter and the 2-norm of a vector, respectively. Once the displacement on the exterior boundary and the COD are obtained by solving (3) and (4), the displacement field on the crack surfaces can be reconstructed by applying the displacement BIE (3) on the crack surface [7, 15].

2.2. Criteria for fatigue crack growth

The growth rate of a fatigue crack is defined by the Paris law [1, 2, 18] as follows:

$$\frac{\mathrm{d}a}{\mathrm{d}N} = C(K_{\mathrm{eq}}^R(\mathbf{u}(\boldsymbol{\chi}), \boldsymbol{\chi}))^m \tag{7}$$

DOI: 10.1002/nme

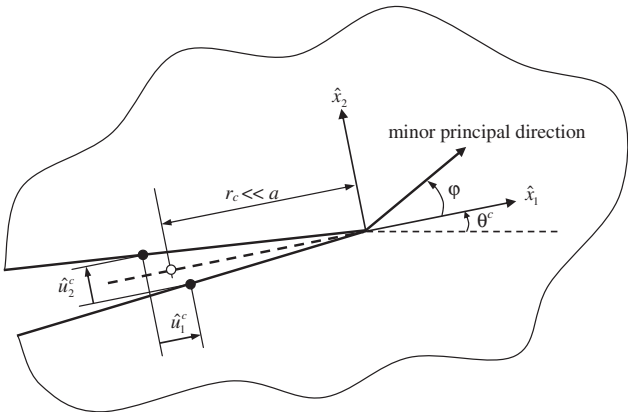

Figure 2. Geometry and local tangent co-ordinate system of crack tip.

where a, N and K_{eq}^R are the crack length, number of load cycles, range of the equivalent stress intensity factor, respectively, while C and m are material constants determined from fatigue tests. The range of the equivalent SIF, $K_{\mathrm{eq}}^R = K_{\mathrm{eq}}^{\max} - K_{\mathrm{eq}}^{\min} = (1 - R)K_{\mathrm{eq}}^{\max}$, where $R = K_{\mathrm{eq}}^{\min}/K_{\mathrm{eq}}^{\max}$. $K_{\mathrm{eq}}^{\max}$ and $K_{\mathrm{eq}}^{\min}$ are the equivalent SIFs corresponding to the maximum and minimum load level, respectively. The equivalent SIF is defined for the mixed-mode fracture as follows [3]:

$$K_{\mathrm{eq}}(\mathbf{u}(\boldsymbol{\chi}), \boldsymbol{\chi}) = K_{\mathrm{I}}(\mathbf{u}(\boldsymbol{\chi}), \boldsymbol{\chi}) \cos^3 \frac{\varphi}{2} - 3K_{\mathrm{II}}(\mathbf{u}(\boldsymbol{\chi}), \boldsymbol{\chi}) \cos^2 \frac{\varphi}{2} \sin \frac{\varphi}{2} \tag{8}$$

where K_{I}, K_{II} and φ are the mode I SIF, the mode II SIF and minor principal direction at the crack tip, respectively, in the local tangent co-ordinate system $(\hat{x}_1, \hat{x}_2)$ shown in Figure 2. In the local tangent co-ordinate system, the crack-tip position and the tangent direction of the crack path at the crack tip are taken as the origin and the $\hat{x}_1$-axis, respectively. Variables with a hat symbol $(\hat{})$ denote those defined in the local tangent co-ordinate system, hereafter. The angle between the global and the local tangent co-ordinate system is denoted as θ^c in Figure 2.

The mixed-mode SIFs are defined by the COD as follows:

$$\mathbf{K}(\mathbf{u}(\boldsymbol{\chi}), \boldsymbol{\chi}) = (K_{\mathrm{II}}(\mathbf{u}(\boldsymbol{\chi}), \boldsymbol{\chi}), K_{\mathrm{I}}(\mathbf{u}(\boldsymbol{\chi}), \boldsymbol{\chi})) = \frac{\mu\sqrt{2\pi}}{\kappa + 1} \lim_{r_c \to 0} \frac{\hat{\mathbf{u}}^c(\boldsymbol{\chi})}{\sqrt{r_c}} = \frac{\mu\sqrt{2\pi}}{\kappa + 1} \lim_{r_c \to 0} \frac{\mathbf{R}^t \mathbf{u}^c(\boldsymbol{\chi})}{\sqrt{r_c}} \tag{9}$$

where μ, r_c, $\hat{\mathbf{u}}^c$ and $\mathbf{R}^t$ are the shear modulus, distance from the crack tip, COD in the local tangent co-ordinate system and rotational matrix from the global to the local co-ordinate system, respectively. For plane strain condition, $\kappa = 3-4\nu$ and for plane stress condition, $\kappa = (3-\nu)/(1+\nu)$, where ν is the Poisson ratio. The minor principal direction at the crack tip in the local tangent co-ordinate is expressed in terms of the mixed-mode SIFs by setting $\partial\sigma_{\theta\theta}/\partial\varphi = 0$, where $\sigma_{\theta\theta}$ is the circumferential stress component near the crack tip [3, 18].

$$\varphi(\mathbf{K}) = \sin^{-1}\left(\frac{K_{\mathrm{II}}}{\sqrt{K_{\mathrm{I}}^2 + 9K_{\mathrm{II}}^2}}\right) - \sin^{-1}\left(\frac{3K_{\mathrm{II}}}{\sqrt{K_{\mathrm{I}}^2 + 9K_{\mathrm{II}}^2}}\right) \tag{10}$$

DOI: 10.1002/nme

Since the shear stress on the principal plane vanishes, the mode II SIF of a crack evaluated in the minor principal direction given in (10) is zero [18]. Here, it should be noted that the minor principal direction in (10) is not changed during a load cycle for the proportional fatigue load, and is considered as a function of the maximum mixed-mode SIFs hereafter.

The fatigue crack length after N load cycles is obtained by integrating the Paris law, and is equal to the arc length of the crack path defined in (2).

$$a = a_0 + \int_0^N C(K_{\mathrm{eq}}^R(\mathbf{u}(\boldsymbol{\chi}), \boldsymbol{\chi}))^m \, \mathrm{d}N = a_0 + \int_{\tau_0}^{\overline{\tau}} \|\boldsymbol{\chi}'(\tau)\|_2 \, \mathrm{d}\tau \tag{11}$$

where a_0 and τ_0 are the initial crack length and its corresponding curve parameter, respectively. The Paris law in (11) is considered as a function of the maximum mixed-mode SIFs only since R is constant through entire load cycles for a proportional cyclic load with constant amplitude.

The PLS is employed to define a curved path of a growing fatigue crack [11, 12, 19]. The PLS states that a crack grows smoothly in the direction of $K_{\mathrm{II}} = 0$, which is the minor principal direction defined in (10). Once a crack grows in accordance with the PLS, the mode II SIF of the crack is always zero in the growing direction, and the minor principal direction given in (10) becomes zero in the local tangent co-ordinate system.

$$\varphi(\mathbf{K}) = 0 \tag{12}$$

Condition (12) implies that a crack grows in the tangential direction of a crack path at the crack tip, and therefore the path of a growing crack is continuous in slope. Cotterell and Rice point out that other criteria for growth direction such as the maximum principal stress criterion or the maximum energy release rate criterion are equivalent to the PLS if a crack grows along a smooth path [19]. Since the tangential direction at the initial crack tip generally does not coincide with the direction of $K_{\mathrm{II}} = 0$ due to the arbitrariness of initial crack geometry, there may be discontinuity in slope by the angle given in (10) at the initial crack tip. The boundary unknowns and the fatigue crack path are obtained by simultaneously solving three non-linear equations, i.e. the BIEs, the Paris law and the PLS.

3. DISCRETIZATION AND INCREMENTAL FORMULATION

The displacement and traction BIEs for a cracked body are discretized by the BEM using straight-line elements, and the incremental crack path is modelled by a parabolic curve defined in the local tangent co-ordinate system for each incremental step. Since the discretized equations of the BIEs and the crack growth criterion are non-linear with respect to the nodal unknowns and the crack-tip position, the iterative forms of the discretized equations are derived to solve the system of non-linear equations by the Newton–Raphson method.

3.1. Discretization of the governing equations

The fatigue crack growth is analysed incrementally for finite sequential increments of load cycles. The crack path for the pth increment of load cycles is parameterized as follows:

$$\boldsymbol{\chi}_p = \boldsymbol{\chi}_{p-1} + \delta\boldsymbol{\chi}_p(\tau) \quad (0 \leqslant \tau \leqslant 1) \tag{13}$$

DOI: 10.1002/nme

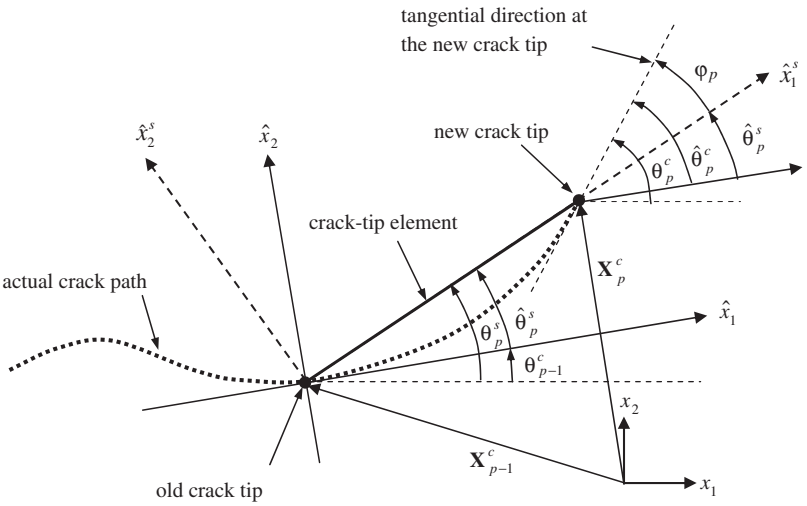

Figure 3. Parabolic modelling of a curved crack path.

where $\delta\boldsymbol{\chi}_p$ is the pth incremental crack path and τ is a curve parameter for the incremental crack path. Each increment of load cycles is referred to as a step for the purpose of brevity. In this paper, each incremental crack path is modelled as a parabola defined in the local tangent co-ordinate system set up at the old crack tip as shown in Figure 3. A parabola, which represents the incremental crack path of the current step, is defined by the new crack-tip position in the local tangent co-ordinate system.

$$\delta\hat{\boldsymbol{\chi}}_p(\tau) = ((\hat{X}_1^c)_p\tau, (\hat{X}_2^c)_p\tau^2) \tag{14}$$

where $\hat{\mathbf{X}}_p^c = ((\hat{X}_1^c)_p, (\hat{X}_2^c)_p)$ is the new crack-tip position for the current step in the local tangent co-ordinate system. The new crack-tip position, $\mathbf{X}_p^c$, and the incremental crack path, $\delta\boldsymbol{\chi}_p(\tau)$, in the global co-ordinate system are given as

$$\mathbf{X}_p^c = \mathbf{X}_{p-1}^c + (\mathbf{R}_{p-1}^t)^{-1}\hat{\mathbf{X}}_p^c \tag{15}$$

$$\delta\boldsymbol{\chi}_p(\tau) = (\mathbf{R}_{p-1}^t)^{-1}\delta\hat{\boldsymbol{\chi}}_p(\tau) \tag{16}$$

where $\mathbf{R}_{p-1}^t$ is the rotational matrix between the global and the local tangent co-ordinate system with a rotational angle θ_{p-1}^c. Since the tangential direction of the incremental crack path at $\tau = 0$ coincides with the $\hat{x}_1$-axis of the local tangent co-ordinate system, the crack path always maintains continuity in slope as required in the PLS.

The BIEs given in (3) and (4) are discretized by the BEM using straight-line boundary elements [7, 10, 15] as shown in Figure 4. The exterior boundary of the cracked body is discretized with continuous quadratic boundary elements, while the crack surface is discretized with discontinuous quadratic boundary elements. Semi-continuous elements [10, 15] are used to connect the exterior boundary to the crack surface for an edge crack. Note that, although the incremental crack path is modelled by a parabola, the incremental crack path is discretized with a straight boundary element for the evaluation of the BIEs [15]. To model the $1/\sqrt{r}$ singularity of the stress field at

DOI: 10.1002/nme

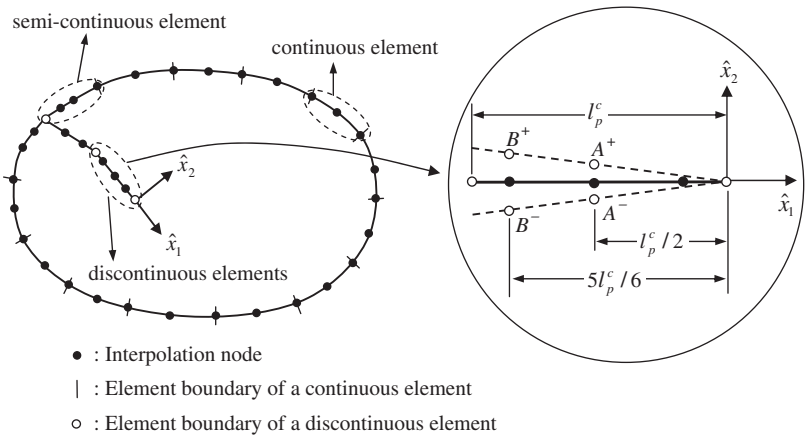

Figure 4. Single-domain boundary discretization of a cracked body.

a crack tip correctly, a singular element has to be utilized. Various types of efficient and accurate singular elements [7, 11] have been proposed. Among them this paper adopts the singular element proposed by Kebir *et al.* [7]. Note that any singular element may be employed as long as it correctly represents the singular field of stress. For each step, one new singular crack-tip element is added to the old crack tip, and the old crack-tip element is replaced with a regular discontinuous element. The boundary integrals for regular elements are integrated analytically. The boundary integrals for the crack-tip element are numerically evaluated by using the 16-point Gauss quadrature when the source is placed outside of the crack-tip element. Analytical integration is performed for the crack-tip element when a source is placed inside of the crack-tip element.

The discretized BIEs (3) and (4) are numerically evaluated and assembled for the maximum load level.

$$\begin{bmatrix} \mathbf{H}_u(\mathbf{X}_p^c) \\ \mathbf{H}_q(\mathbf{X}_p^c) \end{bmatrix} \begin{pmatrix} \mathbf{U}_p^n \\ \mathbf{U}_p^c \end{pmatrix} = \begin{bmatrix} \mathbf{G}_u(\mathbf{X}_p^c) \\ \mathbf{G}_q(\mathbf{X}_p^c) \end{bmatrix} \begin{pmatrix} \mathbf{Q}_p^n \\ \mathbf{0} \end{pmatrix} \quad \text{or} \quad \mathbf{H}(\mathbf{X}_p)\mathbf{U}_p = \mathbf{G}(\mathbf{X}_p)\mathbf{Q}_p \tag{17}$$

where $\mathbf{U}_p^n$ and $\mathbf{U}_p^c$ are the nodal displacements on the exterior boundary and the nodal COD on the crack surface, respectively, and $\mathbf{Q}_p^n$ is the nodal traction on the exterior boundary corresponding to the maximum load level. $\mathbf{H}$ and $\mathbf{G}$ are the system matrices of the discretized BIEs, and subscript u and q denote the displacement and the traction BIE, respectively. Since the crack surface is traction free, the nodal traction corresponding to $\mathbf{U}_p^c$ is set to zero.

For simplicity of presentation, the mixed-mode SIFs that appear in the following formulation denote the maximum mixed-mode SIFs. The Paris law given in (11) is discretized for sequential increments of load cycles.

$$\begin{aligned} a_p &= a_0 + \sum_{l=1}^{p-1} \int_{N_{l-1}}^{N_l} C(K_{\text{eq}}^R(\mathbf{U}_l^c, \mathbf{X}_l^c))^m \, \mathrm{d}N + \int_{N_{p-1}}^{N_p} C(K_{\text{eq}}^R(\mathbf{U}_p^c, \mathbf{X}_p^c))^m \, \mathrm{d}N \\ &= a_0 + \sum_{l=1}^{p-1} \int_0^1 \|\delta\boldsymbol{\chi}_l'(\tau)\|_2 \, \mathrm{d}\tau + \int_0^1 \|\delta\boldsymbol{\chi}_p'(\tau)\|_2 \, \mathrm{d}\tau \end{aligned} \tag{18}$$

DOI: 10.1002/nme

In case the above relation is satisfied up to the previous step, the incremental crack length is equal to the arc length of the incremental crack path.

$$\delta a(\mathbf{U}_p^c, \mathbf{X}_p^c) \equiv \int_{N_{p-1}}^{N_p} C(K_{\mathrm{eq}}^R(\mathbf{U}_p^c, \mathbf{X}_p^c))^m \, \mathrm{d}N = \int_0^1 \|\delta\boldsymbol{\chi}_p'(\tau)\|_2 \, \mathrm{d}\tau \equiv L(\hat{\mathbf{X}}_p^c) \tag{19}$$

where δa and L indicate incremental crack length obtained from the Paris law and the arc length of the incremental crack path. The Paris law and the arc length of the incremental crack path in (19) are evaluated by trapezoidal rule and analytical integration, respectively, which leads to the following expression:

$$\begin{aligned}&\frac{C\Delta N_p}{2}\{(K_{\mathrm{eq}}^R(\mathbf{U}_{p-1}^c, \mathbf{X}_{p-1}^c))^m + (K_{\mathrm{eq}}^R(\mathbf{U}_p^c, \mathbf{X}_p^c))^m\} \\ &= \frac{1}{2}\sqrt{(\hat{X}_1^c)_p^2 + 4(\hat{X}_2^c)_p^2} + \frac{(\hat{X}_1^c)_p^2}{4(\hat{X}_2^c)_p}\left(\ln\left|2(\hat{X}_2^c)_p + \sqrt{(\hat{X}_1^c)_p^2 + 4(\hat{X}_2^c)_p^2}\right| - \ln|(\hat{X}_1^c)_p|\right)\end{aligned} \tag{20}$$

where $\Delta N_p = N_p - N_{p-1}$ is an increment of load cycles or simply referred to as a step size.

The SIFs are evaluated by the displacement extrapolation method using COD [7, 15], which is a finite difference approximation of (9). As the COD at the crack tip is zero, the mixed-mode SIFs can be calculated by the finite difference approximation using the CODs at node A and B in the crack-tip element shown in Figure 4. To obtain more accurate SIFs at the crack tip, the two SIFs approximated at node A and B are extrapolated to the crack tip. The extrapolation scheme employed in this study is originally proposed by Portela *et al*. [15] for a regular quadratic element, and is extended to a singular element by Kebir *et al*. [7]. The detailed derivation of the extrapolation formula is found in Reference [15]. The mixed-mode SIFs for the current step should be calculated in the local tangent co-ordinate system at the new crack tip. Since a straight crack-tip element connecting the new and the old crack tip is used to discretize the BIE, the tangent direction of the new crack-tip element becomes the secant direction between the old and the new crack-tip position. The mixed-mode SIFs evaluated in a local secant co-ordinate system $(\hat{x}_1^s, \hat{x}_2^s)$, which is defined by taking the old crack-tip position as the origin and the secant direction as the local $\hat{x}_1^s$-axis as shown in Figure 3, are given as

$$\mathbf{K}(\mathbf{U}_p^c, \mathbf{X}_p^c) \approx \mathbf{R}_p^s(\mathbf{X}_p^c)(5(\mathbf{U}_A^c)_p - \frac{3\sqrt{15}}{5}(\mathbf{U}_B^c)_p)\frac{\mu}{\kappa+1}\sqrt{\frac{\pi}{l_p^c}} \tag{21}$$

where $\mathbf{U}_A^c$ and $\mathbf{U}_B^c$ are the CODs in the global co-ordinate system at nodes A and B of the crack-tip element as shown in Figures 4, respectively, and $l_p^c = \|\mathbf{X}_p^c - \mathbf{X}_{p-1}^c\|_2$ is the length of the crack-tip element for the current step. The rotation matrix $\mathbf{R}_p^s$ from the global to the local secant co-ordinate system is defined as follows:

$$\mathbf{R}_p^s = \begin{bmatrix} \cos\theta_p^s & \sin\theta_p^s \\ -\sin\theta_p^s & \cos\theta_p^s \end{bmatrix} = \frac{1}{l_p^c}\begin{bmatrix} (X_1^c)_p - (X_1^c)_{p-1} & (X_2^c)_p - (X_2^c)_{p-1} \\ -((X_2^c)_p - (X_2^c)_{p-1}) & (X_1^c)_p - (X_1^c)_{p-1} \end{bmatrix} \tag{22}$$

The PLS is enforced discretely at every newly formed crack tip. Since the mixed-mode SIFs (21) are calculated in the local secant co-ordinate system, the growth direction at the

DOI: 10.1002/nme

new crack tip in the local secant co-ordinate system is given as the angle defined in (10). As shown in Figure 3, the crack growth direction at the new crack tip in the local tangent co-ordinate system is obtained by adding the angle given in (10) to the secant angle of the crack-tip element.

$$\hat{\theta}_p^c(\mathbf{X}_p^c) = \hat{\theta}_p^s(\mathbf{X}_p^c) + \varphi_p(\mathbf{K}(\mathbf{U}_p^c, \mathbf{X}_p^c)) \tag{23}$$

where $\hat{\theta}_p^c$ and $\hat{\theta}_p^s$ are the crack growth angle at the new crack tip and the secant angle of the crack-tip element measured in the local tangent co-ordinate system, respectively. The secant angle in the local tangent co-ordinate system is expressed as follows:

$$\hat{\theta}_p^s(\mathbf{X}_p^c) = \tan^{-1}\left(\frac{(\hat{X}_2^c)_p}{(\hat{X}_1^c)_p}\right) \tag{24}$$

Meanwhile, the tangential direction of the incremental crack path at the new crack tip should be equal to the crack growth direction given in (23) to maintain the smoothness of the crack path as stated in the PLS.

$$\hat{\theta}_p^c(\mathbf{X}_p^c) = \tan^{-1}\left(2\frac{(\hat{X}_2^c)_p}{(\hat{X}_1^c)_p}\right) \tag{25}$$

Substitution of (24) and (25) into (23) leads to the following discretized criterion for crack growth:

$$\varphi_p(\mathbf{K}(\mathbf{U}_p^c, \mathbf{X}_p^c)) = \tan^{-1}\left(2\frac{(\hat{X}_2^c)_p}{(\hat{X}_1^c)_p}\right) - \tan^{-1}\left(\frac{(\hat{X}_2^c)_p}{(\hat{X}_1^c)_p}\right) \equiv \alpha(\hat{\mathbf{X}}_p^c) \tag{26}$$

Three governing equations of (17), (20) and (26) are non-linear with respect to the new crack-tip position and nodal unknowns. To solve the non-linear governing equations, iterative procedure based on the Newton–Raphson method is employed.

3.2. Iterative forms of governing equations

Iterative expressions of the discretized governing equations are derived using the following notation for iterative updates of field variables for the pth step:

$$(\,)_p^k = (\,)_p^{k-1} + \Delta(\,)_p^k = \underline{(\,)} + \Delta(\,) \tag{27}$$

where superscript k denotes the iteration count. The linearized, incremental forms of (17), (20) and (26) are obtained by applying the truncated Taylor expansion with respect to the nodal unknowns and the crack-tip position and including only the first-order terms of the iterative updates.

The discretized BIE (17) is linearized for the iterative updates of nodal unknowns and the new crack-tip position.

$$\mathbf{H}(\underline{\mathbf{X}}^c)\underline{\mathbf{U}} + \mathbf{H}(\underline{\mathbf{X}}^c)\Delta\mathbf{U} + \left(\frac{\partial \mathbf{H}}{\partial \mathbf{X}^c}\underline{\mathbf{U}}\right)\Delta\mathbf{X}^c = \mathbf{G}(\underline{\mathbf{X}}^c)\underline{\mathbf{Q}} + \mathbf{G}(\underline{\mathbf{X}}^c)\Delta\mathbf{Q} + \left(\frac{\partial \mathbf{G}}{\partial \mathbf{X}^c}\underline{\mathbf{Q}}\right)\Delta\mathbf{X}^c \tag{28}$$

DOI: 10.1002/nme

where $\partial\mathbf{H}/\partial\mathbf{X}^c$ and $\partial\mathbf{G}/\partial\mathbf{X}^c$ indicate the sensitivities of $\mathbf{H}$ and $\mathbf{G}$ with respect to the crack-tip position, which are expressed as follows:

$$\frac{\partial\mathbf{H}_u^i}{\partial\mathbf{X}^c} = \sum_e \int_{\Gamma_q^e} \frac{\partial\mathbf{T}^i}{\partial\mathbf{X}^c}\mathbf{N}_u^e \,\mathrm{d}\Gamma + \sum_e \int_{s_c^e} \left(\frac{\partial\mathbf{T}^i}{\partial\mathbf{X}^c}\mathbf{N}_u^e J + \mathbf{T}^i\mathbf{N}_u^e \frac{\partial J}{\partial\mathbf{X}^c} \right) \mathrm{d}\tau$$

$$\frac{\partial\mathbf{G}_u^i}{\partial\mathbf{X}^c} = \sum_e \int_{\Gamma_u^e} \frac{\partial\mathbf{S}^i}{\partial\mathbf{X}^c}\mathbf{N}_q^e \,\mathrm{d}\Gamma + \sum_e \int_{\Gamma_q^e} \frac{\partial\mathbf{S}^i}{\partial\mathbf{X}^c}\mathbf{N}_q^e \,\mathrm{d}\Gamma$$

$$\frac{\partial\mathbf{H}_q^i}{\partial\mathbf{X}^c} = \frac{\partial\mathbf{n}_s^i}{\partial\mathbf{X}^c} \cdot \left(\sum_e \int_{\Gamma_q^e} (\mathbf{T}^\sigma)^i \mathbf{N}_u^e \,\mathrm{d}\Gamma + \sum_e \oint_{s_c^e} (\mathbf{T}^\sigma)^i \mathbf{N}_u^e \,\mathrm{d}\tau \right) + \mathbf{n}_s^i \cdot \sum_e \int_{\Gamma_q^e} \frac{\partial(\mathbf{T}^\sigma)^i}{\partial\mathbf{X}^c}\mathbf{N}_u^e \,\mathrm{d}\Gamma$$
$$+ \mathbf{n}_s^i \cdot \sum_e \oint_{s_c^e} \left(\frac{\partial(\mathbf{T}^\sigma)^i}{\partial\mathbf{X}^c}\mathbf{N}_u^e J + (\mathbf{T}^\sigma)^i \mathbf{N}_u^e \frac{\partial J}{\partial\mathbf{X}^c} \right) \mathrm{d}\tau$$

$$\frac{\partial\mathbf{G}_q^i}{\partial\mathbf{X}^c} = \frac{\partial\mathbf{n}_s^i}{\partial\mathbf{X}^c} \cdot \left(\sum_e \int_{\Gamma_u^e} (\mathbf{S}^\sigma)^i \mathbf{N}_q^e \,\mathrm{d}\Gamma + \sum_e \int_{\Gamma_q^e} (\mathbf{S}^\sigma)^i \mathbf{N}_q^e \,\mathrm{d}\Gamma \right)$$
$$+ \mathbf{n}_s^i \cdot \left(\sum_e \int_{\Gamma_u^e} \frac{\partial(\mathbf{S}^\sigma)^i}{\partial\mathbf{X}^c}\mathbf{N}_q^e \,\mathrm{d}\Gamma + \sum_e \int_{\Gamma_q^e} \frac{\partial(\mathbf{S}^\sigma)^i}{\partial\mathbf{X}^c}\mathbf{N}_q^e \,\mathrm{d}\Gamma \right) \tag{29}$$

where $\mathbf{N}_u^e$, $\mathbf{N}_q^e$, $\sum_e$ and s_c^e are the shape functions for displacement and traction, the assembly operator of the BEM and the discretized crack paths, respectively, and the BIEs and variables with the superscript i correspond to those when a source is applied at node i. Since sources are applied only on the exterior boundary in the displacement BIE, the sensitivity of the jump term of the displacement at a source point vanishes. Refer to Appendix A.2 for the detailed forms of the sensitivities of the kernel functions, the normal vectors and the Jacobian. Tai and Fenner [20] have presented explicit expressions of the sensitivities of the displacement BIE. Note that the sensitivity of the Jacobian exists only on the crack-tip element and is expressed in terms of the crack-tip position. In case the solutions obtained by the previous iteration satisfy the BIE, the linearized form (28) becomes as follows:

$$\mathbf{H}(\underline{\mathbf{X}}^c)\Delta\mathbf{U} + \left(\frac{\partial\mathbf{H}}{\partial\mathbf{X}^c}\,\underline{\mathbf{U}} \right) \Delta\mathbf{X}^c = \mathbf{G}(\underline{\mathbf{X}}^c)\Delta\mathbf{Q} + \left(\frac{\partial\mathbf{G}}{\partial\mathbf{X}^c}\,\underline{\mathbf{Q}} \right) \Delta\mathbf{X}^c \tag{30}$$

The linearized forms of the discretized Paris law (20) and the PLS (26) are derived in terms of the iterative updates of the COD and the new crack-tip position.

$$\frac{C\Delta N_p}{2} \left\{ (K_{\mathrm{eq}}^R(\mathbf{U}_{p-1}, \mathbf{X}_{p-1}^c))^m + (\underline{K}_{\mathrm{eq}}^R)^m + m(\underline{K}_{\mathrm{eq}}^R)^{m-1} \left(\frac{\partial K_{\mathrm{eq}}^R}{\partial\mathbf{K}} \frac{\partial\mathbf{K}}{\partial\mathbf{U}^c}\Delta\mathbf{U}^c \right.\right.$$
$$\left.\left. + \frac{\partial K_{\mathrm{eq}}^R}{\partial\mathbf{K}} \frac{\partial\mathbf{K}}{\partial\mathbf{X}^c}\Delta\mathbf{X}^c \right) \right\} = \underline{L} + \frac{\partial L}{\partial\hat{\mathbf{X}}^c}\mathbf{R}_{p-1}^t \Delta\mathbf{X}^c \tag{31}$$

$$\underline{\varphi} + \frac{\partial\varphi}{\partial\mathbf{K}} \frac{\partial\mathbf{K}}{\partial\mathbf{U}^c}\Delta\mathbf{U}^c + \frac{\partial\varphi}{\partial\mathbf{K}} \frac{\partial\mathbf{K}}{\partial\mathbf{X}^c}\Delta\mathbf{X}^c = \underline{\alpha} + \frac{\partial\alpha}{\partial\hat{\mathbf{X}}^c}\mathbf{R}_{p-1}^t \Delta\mathbf{X}^c \tag{32}$$

DOI: 10.1002/nme

where $\underline{K}^R_{\mathrm{eq}} = K^R_{\mathrm{eq}}(\underline{\mathbf{U}}, \underline{\mathbf{X}}^c)$, $\underline{L} = L(\underline{\mathbf{X}}^c)$, $\underline{\varphi} = \varphi(\mathbf{K}(\underline{\mathbf{U}}^c, \underline{\mathbf{X}}^c))$ and $\underline{\alpha} = \alpha(\underline{\mathbf{X}}^c)$. The derivatives of L and α with respect to $\hat{\mathbf{X}}^c$ are given in Appendix A.3. The derivatives of K^R_{eq} and φ with respect to SIFs in (31) and (32) are obtained by the direct differentiation of (8) and (10), respectively, and presented in Appendix A.4. Terms containing $\partial K^R_{\mathrm{eq}}/\partial\varphi$ do not appear in (31) because the condition of $\partial\sigma_{\theta\theta}/\partial\varphi = 0$ used to derive the minor principal direction (10) is equivalent to $\partial K^R_{\mathrm{eq}}/\partial\varphi = 0$ [3, 18].

Direct differentiation of (21) with respect to the COD and the crack-tip position leads to the following expressions for the sensitivities of the mixed-mode SIFs:

$$\frac{\partial \mathbf{K}}{\partial \mathbf{U}^c}\Delta\mathbf{U}^c = \frac{\partial \mathbf{K}}{\partial \mathbf{U}^c_A}\Delta\mathbf{U}^c_A + \frac{\partial \mathbf{K}}{\partial \mathbf{U}^c_B}\Delta\mathbf{U}^c_B = \mathbf{R}^s_p(\underline{\mathbf{X}})\left(5\Delta\mathbf{U}^c_A - \frac{3\sqrt{15}}{5}\Delta\mathbf{U}^c_B\right)\frac{\mu}{\kappa+1}\sqrt{\frac{\pi}{\underline{l}^c}} \tag{33}$$

$$\frac{\partial \mathbf{K}}{\partial \mathbf{X}^c} = \frac{\partial \mathbf{R}^s_p}{\partial \mathbf{X}^c}\left(5\underline{\mathbf{U}}^c_A - \frac{3\sqrt{15}}{5}\underline{\mathbf{U}}^c_B\right)\frac{\mu}{\kappa+1}\sqrt{\frac{\pi}{\underline{l}^c}} - \mathbf{R}^s_p(\underline{\mathbf{X}})\left(5\underline{\mathbf{U}}^c_A - \frac{3\sqrt{15}}{5}\underline{\mathbf{U}}^c_B\right)$$
$$\times\frac{\mu}{\kappa+1}\frac{\sqrt{\pi}}{2\underline{l}^c\sqrt{\underline{l}^c}}\frac{\partial l^c_p}{\partial \mathbf{X}^c} \tag{34}$$

where $\partial l^c_p/\partial\mathbf{X}^c = (\underline{\mathbf{X}}^c - \mathbf{X}^c_{p-1})/\underline{l}^c$ and $\partial\mathbf{R}^s_p/\partial\mathbf{X}^c$ is derived by the direct differentiation of (22).

$$\frac{\partial \mathbf{R}^s_p}{\partial X^c_1} = \frac{1}{\underline{l}^c}\left(\mathbf{I} - \frac{\partial l^c_p}{\partial X^c_1}\mathbf{R}^s_p\right), \quad \frac{\partial \mathbf{R}^s_p}{\partial X^c_2} = \frac{1}{\underline{l}^c}\left(\mathbf{I}_a - \frac{\partial l^c_p}{\partial X^c_2}\mathbf{R}^s_p\right) \tag{35}$$

where $\mathbf{I}$ is the identity matrix, and $\mathbf{I}_a$ is defined as

$$\mathbf{I}_a = \begin{bmatrix} 0 & 1 \\ -1 & 0 \end{bmatrix} \tag{36}$$

The nodal unknowns and the crack-tip position are determined by solving (30), (31) and (32) iteratively for each increment of the load cycles. The solution of the linearized equations at each iteration does not precisely satisfy the BIEs. Since, however, the mixed-mode SIFs should be evaluated by the displacement field that satisfies the BIEs exactly for the given crack geometry, the displacement field is updated by solving (17) for the new crack-tip position obtained by solving the linearized equations. The mixed-mode SIFs are calculated using the updated displacement field for the next iteration.

4. NUMERICAL EXAMPLES

The validity of the proposed incremental formulation is demonstrated through two numerical examples on the prediction of fatigue crack growth in plates with initial edge cracks under the plane stress condition. In the examples, results obtained by the proposed method are compared with those obtained by the conventional tangent approach. In the tangent approach, the BIEs are solved for the fixed crack path determined by the SIFs using the previous crack path without iterative correction.

DOI: 10.1002/nme

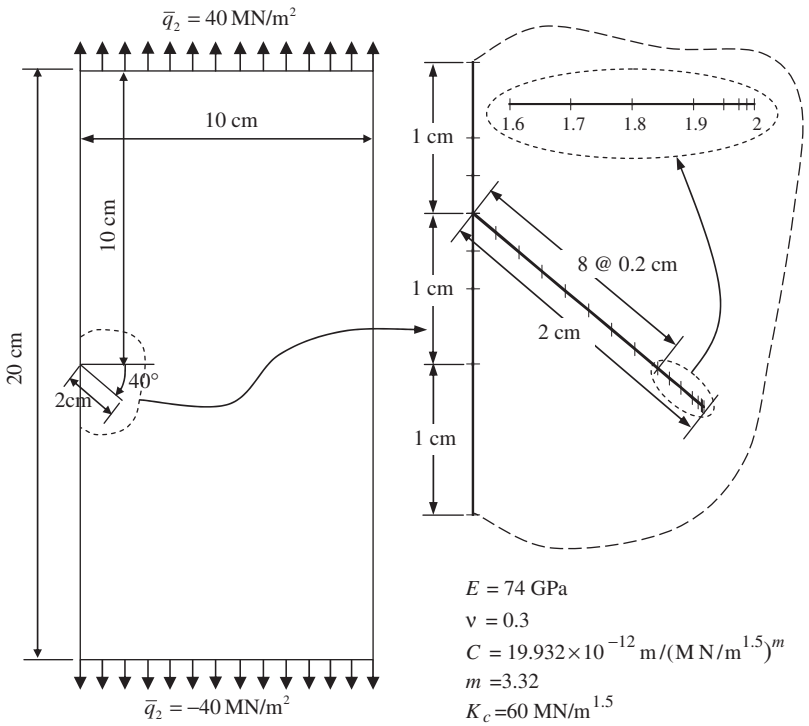

Figure 5. Inclined edge-cracked plate under tensile load and discretization of initial crack.

An incremental crack length corresponding to a fixed increment of load cycles becomes longer as a crack grows because the equivalent SIF increases very fast with crack length. To prevent numerical instability or inaccuracy of solutions caused by an excessive incremental crack length, a step size is reduced by half of the previous one in case an incremental crack length exceeds a prescribed value, $\delta a_{\max}$. The convergence criterion for iterations is selected as follows:

$$\frac{\|\Delta \mathbf{X}^c\|_2}{\|\mathbf{X}_p^c\|_2} < 10^{-7} \tag{37}$$

4.1. Fatigue crack growth in a rectangular plate under a tensile load

The rectangular plate with an inclined edge crack presented in Reference [9] is chosen as a first example to verify the proposed method. The initial geometry, loading condition and material properties are given in Figure 5. The fatigue crack grows from the initial crack of 2 cm inclined by 40° to the horizontal direction. A constant cyclic tension, which ranges from 0 to 40 $\mathrm{MN/m^2}$, is applied on the upper and lower side of the plate. The plate with the initial crack is modelled with 174 nodes and 79 boundary elements. The exterior boundary is discretized with 1 cm elements and the initial crack is discretized with 15 elements, of which sizes gradually decrease from 0.2 at the edge to 0.0125 cm at the crack tip. The detailed mesh layout around the initial crack is

DOI: 10.1002/nme

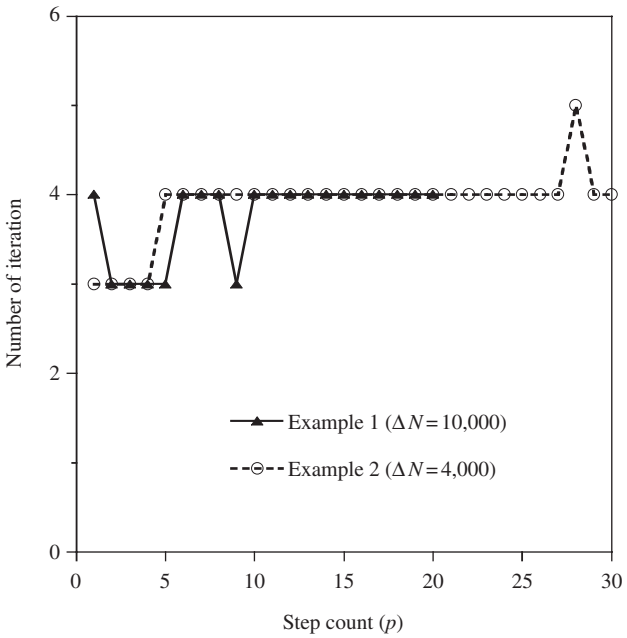

Figure 6. Number of iterations of Examples 1 and 2.

presented in Figure 5. Results obtained by the tangent approach and the proposed method are compared with those by Duflot and Nguyen-Dang [9], in which the meshless Galerkin method is used for the analysis of the cracked body. In their study, the fatigue crack grows by constant increments of 0.5 cm, and the growth direction is determined based on the maximum principal stress criterion using the previous crack-tip position without iterative modification. The number of load cycles required for each crack increment is evaluated by integrating the Paris law (7) with the trapezoidal rule.

The fatigue crack growth is simulated by the proposed method and the tangent approach with $\Delta N = 200$ and 10 000. The simulation is terminated when the total crack length reaches to 6.5 cm, and the maximum incremental crack length is set to 0.5 cm for the reduction of ΔN. Total steps of 588, 19 in the tangent approach and 593, 20 in the proposed method are required for $\Delta N = 200$ and 10 000, respectively. No reduction of ΔN is made in the tangent approach with $\Delta N = 200$ and one reduction occurs at the 592nd step in the proposed method with $\Delta N = 200$. For $\Delta N = 10\,000$, the first reduction occurs at the 13th step in the tangent approach, and at the 11th step in the proposed method. This is because the tangent approach predicts shorter incremental crack length than the proposed method. Figures 6 and 7 present the number of iterations required to converge to the specified criterion for each step and the relative error of each iteration at the 1st step, respectively, in the proposed method for $\Delta N = 10\,000$. The proposed method satisfies the specified criterion after 3 or 4 iterations with quadratic convergence rate for all steps.

Figures 8 and 9 show the predicted growth paths of fatigue crack and SIFs, respectively. The initial mode I and mode II SIFs are calculated as 8.95 and 4.02 $\mathrm{MN/m^{1.5}}$, respectively. After a

DOI: 10.1002/nme

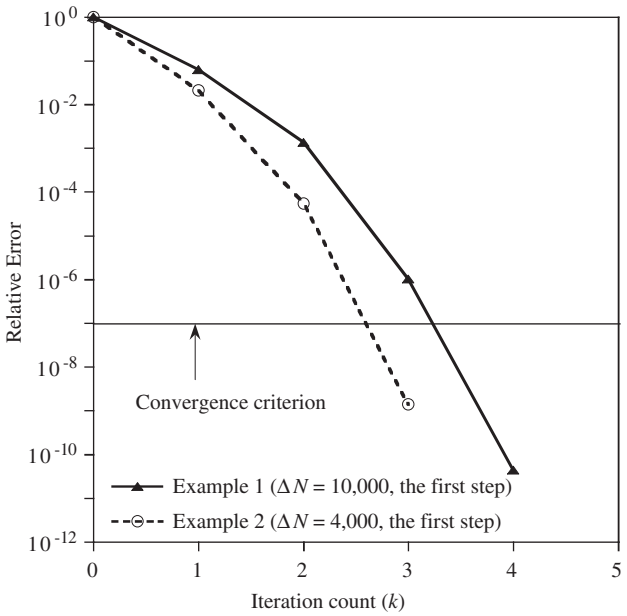

Figure 7. Relative errors at the 1st step of Examples 1 and 2.

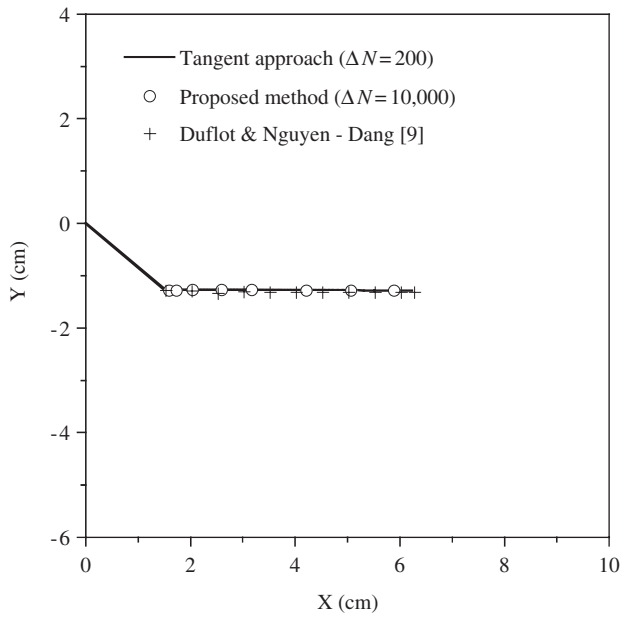

Figure 8. Predicted growth paths of fatigue crack of Example 1.

DOI: 10.1002/nme

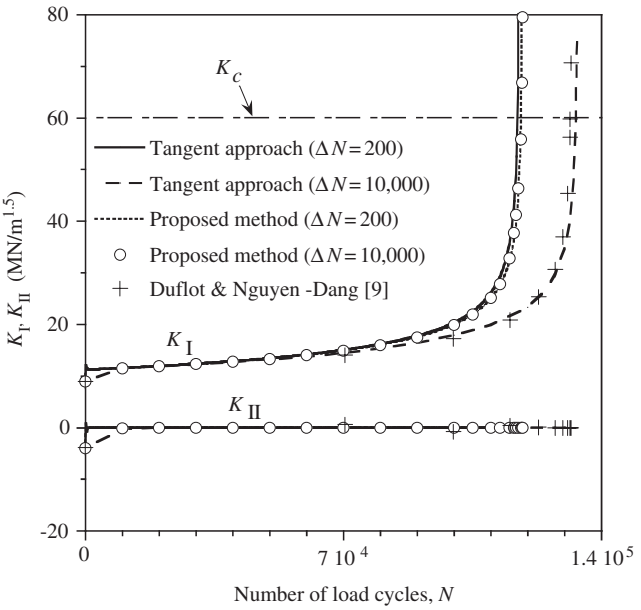

Figure 9. Stress intensity factors for Example 1.

crack initiates growth, the mode II SIF becomes zero as the applied criterion enforces the crack to grow in such a direction. The initial mixed-mode SIFs have the initial crack grow to the direction of 38° from the initial crack, which is almost in a horizontal direction. Since the minor principal direction near the horizontal crack becomes perpendicular to the applied tension, the fatigue crack grows to the horizontal direction after the initial kinks. Therefore, the correction on the direction of crack growth is rarely required, and no significant difference is found in the predicted crack paths among the three approaches.

Significant differences among the three approaches in the SIFs and the crack length *vs* the number of load cycles, however, are found in Figures 9 and 10, respectively. The solutions obtained by the proposed method and the tangent approach for $\Delta N = 200$ are very close to each other because of the small step size. The proposed method yields almost identical results for $\Delta N = 200$ and 10 000. However, the tangent approach with $\Delta N = 10\,000$ underestimates the SIF and the crack length for a given number of load cycles, which is similar to the results by Duflot and Nguyen-Dang [9]. As the load cycles increase, the SIF and the crack length predicted by the tangent approach with $\Delta N = 10\,000$ deviate significantly from those by the proposed method.

It is of great engineering importance to predict the fatigue life correctly. Since the mode II SIF is almost zero for growing crack, the fatigue life is governed by the mode I SIF. The fatigue life for the fracture toughness of 60 MN/m$^{1.5}$ is estimated as 118 250 and 133 130 cycles by the proposed method and the tangent approach with $\Delta N = 10\,000$, which represents a 12.5% difference. When the total number of load cycles reaches to the fatigue life by the proposed method, the SIF and the crack length predicted by the tangent approach with $\Delta N = 10\,000$ are only about 38 and 61% of those predicted by the proposed method, respectively.

DOI: 10.1002/nme

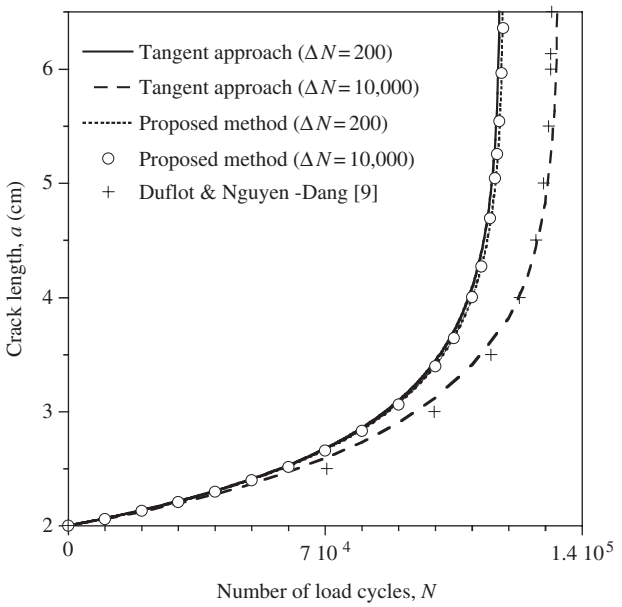

Figure 10. Crack length *vs* load cycles for Example 1.

4.2. Fatigue crack growth in a square plate under a mode II fatigue load

The fatigue crack growth in a 20 cm × 20 cm square plate is investigated for a mode II fatigue load. Figure 11 shows the geometry, boundary conditions and material properties of the plate. Typical material properties of the Ferrite-Pearlite steel [2] are adopted. Mode II fatigue traction that ranges from 0 to 165 MN/m^2 is applied on the upper- and lower-left edge of the plate in the opposite direction. Four different cases of 1, 2, 4 and 8 cm initial cracks are considered. The plates with 1, 2, 4 and 8 cm initial crack are modelled with 199, 214, 244 and 304 nodes and 94, 99, 109 and 129 elements, respectively. The exterior boundary is discretized with 1 cm continuous elements. The element sizes on the crack surface gradually decrease from 0.2 cm at the edge to 0.0125 cm at the crack tip. The mesh layout for the plate with a 1 cm initial crack is presented in Figure 11.

The fatigue crack growth is simulated by the proposed method with $\Delta N = 4000$, 1400, 450 and 124 cycles for 1, 2, 4 and 8 cm initial cracks, respectively, to have the initial cracks grow with similar increments of around 0.056 cm. The maximum incremental crack length for the reduction of ΔN is set to 0.5 cm. In case total crack length for the plate with 1, 2, 4, and 8 cm initial crack reaches to 8, 10, 11 and 15 cm, respectively, the simulation is terminated to prevent the separation of the plate. Total steps of 30, 32, 35 and 36 are made before termination for 1, 2, 4 and 8 cm initial cracks, respectively. The first reduction of ΔN occurs at the 11th, 18th, 23rd and 25th step for 1, 2, 4 and 8 cm initial cracks, respectively. As shown in Figures 6 and 7 for 1 cm initial crack, the proposed method converges quadratically to the specified criterion within four or five iterations.

Figure 12 shows the growth paths of the four different initial cracks. The growth path of the 1 cm initial crack forms a sharp curve with a small radius of curvature. The growth direction changes towards the left edge from the lower edge of the plate at around the 20th step, which can be explained as follows. The mode I and mode II SIF for the initial crack are calculated as 26.22 and

DOI: 10.1002/nme

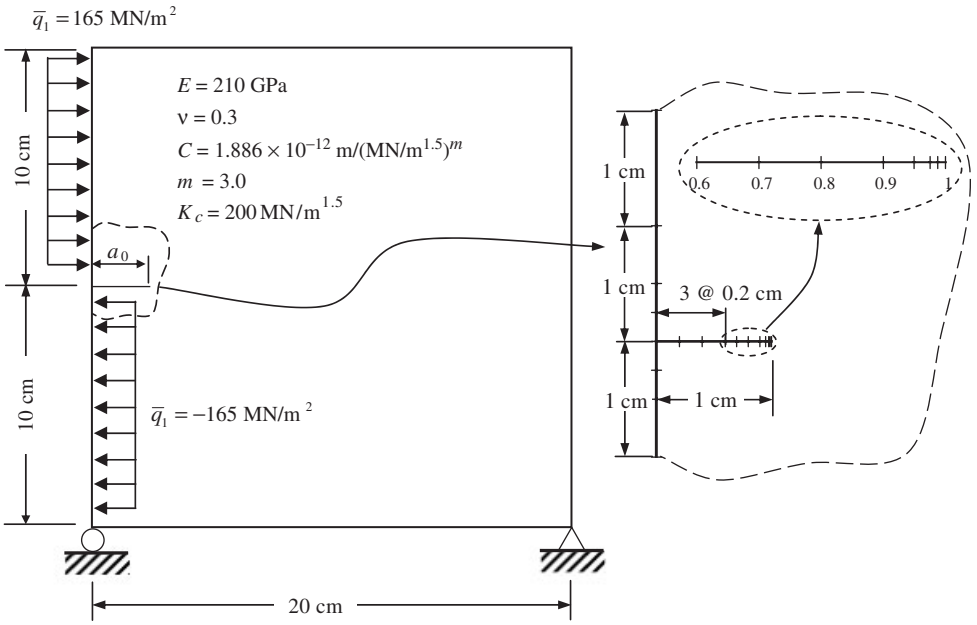

Figure 11. Edge-cracked plate under a mode II load and discretization of initial crack.

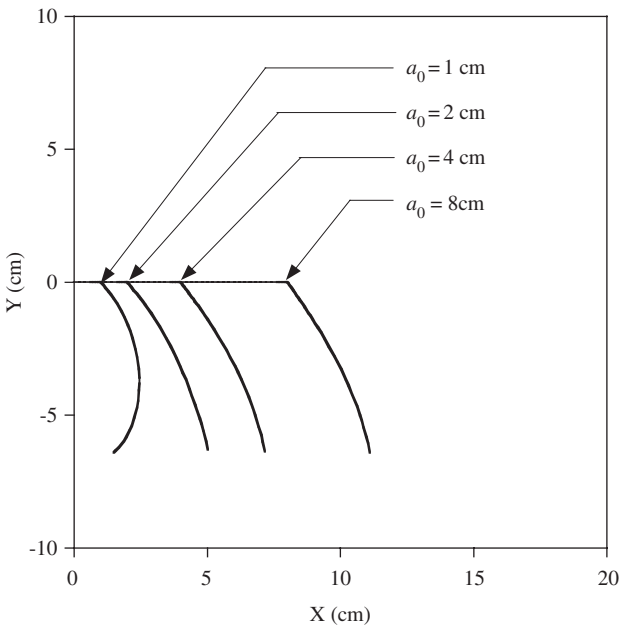

Figure 12. Growth paths for 1, 2, 4 and 8 cm initial cracks of Example 2.

DOI: 10.1002/nme

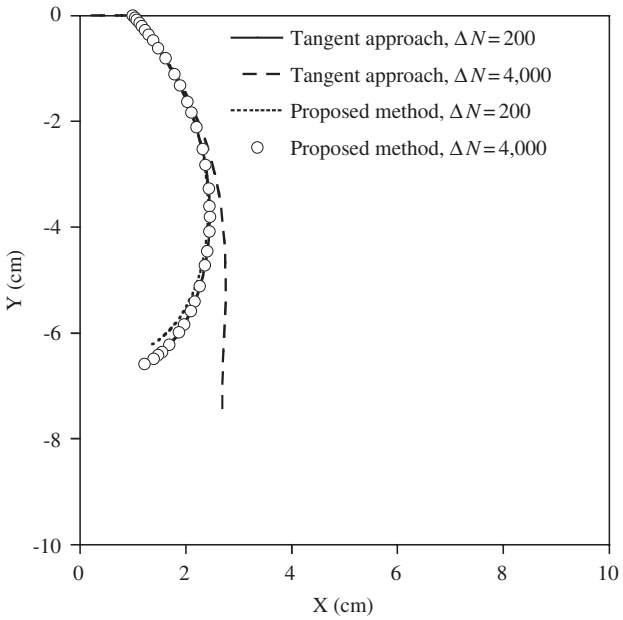

Figure 13. Predicted growth paths for 1 cm initial crack of Example 2.

21.63 $MN/m^{1.5}$, respectively, which has the initial crack kink by 50° from the horizontal direction. As the crack grows after the initial kink, the crack turns the direction of its growth vertically, which is perpendicular to the applied traction, according to the PLS. As the crack grows further, the crack turns the direction of its growth towards the left edges of the plate due to the vertical tension field generated by cantilever-like actions of the left part of the crack. Meanwhile, the other initial cracks grow by relatively dull curves, and maintain the growth direction towards the lower edge of the plate. This is because the cantilever-like actions in the left part of the crack become weaker for the longer initial cracks.

The behaviours of fatigue crack growth are presented in detail for the plate with 1 cm initial crack to demonstrate the efficiency of the proposed method in comparison with the tangent approach. The results obtained by $\Delta N = 200$ and $\delta a_{\max} = 0.1$ cm are chosen as the reference solutions for both methods. Figures 13–15 show the growth paths, SIFs and crack length *vs* number of load cycles, respectively. In the figures, it is clearly seen that the proposed method yields almost identical results regardless of the step size, while the accuracy of the tangent approach heavily depends on the step size. Unlike the previous example, the crack growth path predicted by the tangent approach with $\Delta N = 4000$ exhibits significant differences from the others. Because no correction on the crack growth direction is made for each step in the tangent approach, the crack keeps growing in an incorrect direction once the erroneous growth direction is estimated. As shown in Figure 14, fatigue life for the fracture toughness of 200 $MN/m^{1.5}$ is estimated as 48 250 and 48 630 cycles by the proposed method and the tangent approach with $\Delta N = 200$, respectively, which are very close to each other. The differences in the estimated fatigue life between $\Delta N = 4000$ and 200 are 12.6% for the tangent approach and virtually 0% for the proposed method. As the load cycle increases, huge errors in the SIF and crack length for a given load cycle occur in the tangent approach with

DOI: 10.1002/nme

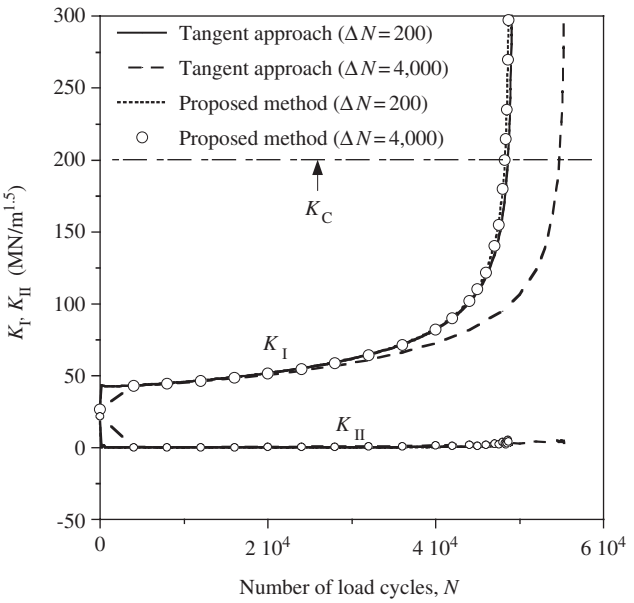

Figure 14. Stress intensity factors of Example 2.

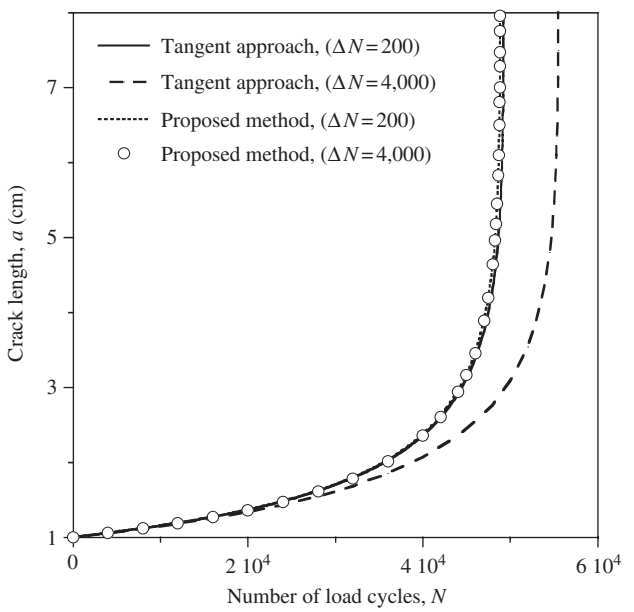

Figure 15. Crack length *vs* load cycles of Example 2.

DOI: 10.1002/nme

a large step size. To obtain reliable results in the tangent approach, the step size should be kept very small. On the other hand, the proposed method yields accurate results even for a large step size.

5. CONCLUSIONS

A new incremental formulation is presented for predicting the curved growth path of a two-dimensional fatigue crack. A cracked body and a crack path are modelled using the displacement and traction BIEs and a parametric form of a curve, respectively. The Paris law and the PLS are employed to define the growth path of a crack. Iterative forms of three governing equations, i.e. the BIEs, the Paris law and the PLS, are derived with respect to the unknown displacement, traction and the crack-tip position. An incremental crack path is discretized by a parabolic curve. The Paris law is integrated by the trapezoidal rule. An iterative solution scheme based on the Newton–Raphson method is presented.

The validity of the proposed method is demonstrated by two numerical examples of plates with an edge crack under the plane stress condition. In the examples, the growth paths and fatigue life predicted by the proposed method are compared with those by the tangent approaches. The proposed method yields accurate and stable solutions, and converges very fast within four or five iterations even for a large step size. It is believed that the proposed method provides a rigorous formulation for the analysis of fatigue crack growth, which is also applicable to domain discretization schemes such as the extended FEM and the element-free Galerkin method.

Although only the fatigue crack growth for two-dimensional edge cracks is presented as examples in this paper, the proposed method can be easily extended to problems of multiple edge or embedded cracks without modification of the basic formulation. In three-dimensional problems the growth direction and length at a point on a crack front may be defined in the normal plane to the tangent of the crack front as presented by Dell'Erba and Aliabadi [8]. Therefore, the proposed method can be applied in the normal plane at each node on the crack front to derive incremental expressions of the three-dimensional crack growth criteria.

APPENDIX A

A.1. Kernels of displacement and traction BIEs

The Kernels of displacement and traction BIEs for two-dimensional elastostatic problems [16, 17] are defined in tensor notation as follows:

$$S_{ij} = \frac{1}{8\pi\mu(1-\nu)} \left\{ \frac{r_i r_j}{r^2} - (3-4\nu)\delta_{ij} \ln r \right\} \tag{A1}$$

$$T_{ij} = -\frac{1}{4\pi(1-\nu)} \frac{1}{r^2} \left\{ r_l n_l \left((1-2\nu)\delta_{ij} + 2\frac{r_i r_j}{r^2} \right) + (1-2\nu)(n_i r_j - n_j r_i) \right\} \tag{A2}$$

$$S^{\sigma}_{ijk} = \frac{1}{4\pi(1-\nu)} \frac{1}{r^2} \left\{ (1-2\nu)(\delta_{ik} r_j + \delta_{jk} r_i - \delta_{ij} r_k) + 2\frac{r_i r_j r_k}{r^2} \right\} \tag{A3}$$

DOI: 10.1002/nme

$$T^{\sigma}_{ijk} = \frac{\mu}{2\pi(1-\nu)}\frac{1}{r^2}\left\{2\frac{r_l n_l}{r^2}\left((1-2\nu)\delta_{ij}r_k + \nu(\delta_{ik}r_j + \delta_{jk}r_i) - 4\frac{r_i r_j r_k}{r^2}\right)\right.$$
$$\left. + 2\nu\left(n_i\frac{r_j r_k}{r^2} + n_j\frac{r_i r_k}{r^2}\right) + (1-2\nu)\left(2n_k\frac{r_i r_j}{r^2} + n_j\delta_{ik} + n_i\delta_{jk}\right) - (1-4\nu)n_k\delta_{ij}\right\} \tag{A4}$$

where μ and δ_{ij} are the shear modulus and Kronecker delta, respectively. On the exterior boundary, r_i is the component of $\mathbf{r} = \mathbf{x} - \boldsymbol{\xi}$ corresponding to global co-ordinate components x_i and r is the distance between $\mathbf{x}$ and $\boldsymbol{\xi}$. On the crack surface, $\boldsymbol{\chi}$ is used instead of $\mathbf{x}$. The outward normal vector of boundary, $\mathbf{n}$, is defined as follows:

$$\mathbf{n} = (n_1, n_2) = \frac{1}{J}\left(\frac{\mathrm{d}x_2}{\mathrm{d}\eta}, -\frac{\mathrm{d}x_1}{\mathrm{d}\eta}\right) \tag{A5}$$

where η and J are the natural co-ordinate of boundary and the Jacobian of transformation from global to natural co-ordinate system of boundary, respectively.

$$J = \sqrt{\left(\frac{\mathrm{d}x_1}{\mathrm{d}\eta}\right)^2 + \left(\frac{\mathrm{d}x_2}{\mathrm{d}\eta}\right)^2} \tag{A6}$$

A.2. Derivatives of kernels of BIEs with respect to crack-tip position

The derivatives of kernels (A1)–(A4) with respect to a crack-tip position is only considered in case that $\boldsymbol{\chi}$ or $\boldsymbol{\xi}$ is on the crack-tip element in this paper.

$$S_{ij,m} = \frac{1}{8\pi\mu(1-\nu)}\left\{\frac{r_{i,m}r_j}{r^2} + \frac{r_i r_{j,m}}{r^2} - 2\frac{r_i r_j r_{,m}}{r^3} - (3-4\nu)\delta_{ij}\frac{r_{,m}}{r}\right\} \tag{A7}$$

$$T_{ij,m} = -\frac{1}{4\pi(1-\nu)}\frac{1}{r^2}\left\{(r_{l,m}n_l + r_l n_{l,m})\left((1-2\nu)\delta_{ij} + 2\frac{r_i r_j}{r^2}\right)\right.$$
$$+ 2r_l n_l\left(\frac{r_{i,m}r_j}{r^2} + \frac{r_i r_{j,m}}{r^2} - 2\frac{r_i r_j r_{,m}}{r^3}\right)$$
$$\left. + (1-2\nu)(n_{i,m}r_j + n_i r_{j,m} - n_{j,m}r_i - n_j r_{i,m})\right\} - 2\frac{r_{,m}}{r}T_{ij} \tag{A8}$$

$$S^{\sigma}_{ijk,m} = \frac{1}{4\pi(1-\nu)}\frac{1}{r^2}\left\{(1-2\nu)(\delta_{ik}r_{j,m} + \delta_{jk}r_{i,m} - \delta_{ij}r_{k,m})\right.$$
$$\left. + 2\frac{r_{i,m}r_j r_k}{r^2} + 2\frac{r_i r_{j,m}r_k}{r^2} + 2\frac{r_i r_j r_{k,m}}{r^2} - 4\frac{r_i r_j r_k}{r^3}r_{,m}\right\} - 2\frac{r_{,m}}{r}S^{\sigma}_{ijk} \tag{A9}$$

DOI: 10.1002/nme

$$T^{\sigma}_{ijk,m} = \frac{\mu}{2\pi(1-\nu)}\frac{1}{r^2}\left\{2\left(\frac{r_{l,m}n_l}{r^2}+\frac{r_l n_{l,m}}{r^2}-2\frac{r_l n_l r_{,m}}{r^3}\right)\left((1-2\nu)\delta_{ij}r_k+\nu(\delta_{ik}r_j+\delta_{jk}r_i)\right.\right.$$

$$\left.-4\frac{r_i r_j r_k}{r^2}\right)+2\frac{r_l n_l}{r^2}((1-2\nu)\delta_{ij}r_{k,m}+\nu(\delta_{ik}r_{j,m}+\delta_{jk}r_{i,m}))$$

$$-8\frac{r_l n_l}{r^2}\left(\frac{r_{i,m}r_j r_k}{r^2}+\frac{r_i r_{j,m}r_k}{r^2}+\frac{r_i r_j r_{k,m}}{r^2}-2\frac{r_i r_j r_k r_{,m}}{r^3}\right)-4\nu\frac{r_{,m}}{r^3}(n_i r_j r_k+n_j r_i r_k)$$

$$+2\nu\frac{1}{r^2}(n_{i,m}r_j r_k+n_i r_{j,m}r_k+n_i r_j r_{k,m}+n_{j,m}r_i r_k+n_j r_{i,m}r_k+n_j r_i r_{k,m})$$

$$+(1-2\nu)\left(2n_{k,m}\frac{r_i r_j}{r^2}+2n_k\frac{r_{i,m}r_j}{r^2}+2n_k\frac{r_i r_{j,m}}{r^2}-4n_k\frac{r_i r_j r_{,m}}{r^3}+n_{j,m}\delta_{ik}+n_{i,m}\delta_{jk}\right)$$

$$\left.-(1-4\nu)n_{k,m}\delta_{ij}\right\}-2\frac{r_{,m}}{r}T^{\sigma}_{ijk} \tag{A10}$$

where commas (,) in the subscripts indicate the derivatives with respect to the co-ordinates of a crack-tip position. The derivatives of r_i, r, $\mathbf{n}$ and J are derived by direct differentiation as follows:

$$r_{i,m} = \chi_{i,m} - \xi_{i,m} \tag{A11}$$

$$r_{,m} = \frac{r_m r_{m,m}}{r} \text{ (here, } m \text{ is a free index)} \tag{A12}$$

$$n_{1,m} = -\frac{J_{,m}}{J^2}\frac{\mathrm{d}\chi_2}{\mathrm{d}\eta}+\frac{1}{J}\frac{\mathrm{d}\chi_{2,m}}{\mathrm{d}\eta}, \quad n_{2,m} = \frac{J_{,m}}{J^2}\frac{\mathrm{d}\chi_1}{\mathrm{d}\eta}-\frac{1}{J}\frac{\mathrm{d}\chi_{1,m}}{\mathrm{d}\eta} \tag{A13}$$

$$J_{,m} = \frac{1}{J}\left(\frac{\mathrm{d}\chi_{1,m}}{\mathrm{d}\eta}+\frac{\mathrm{d}\chi_{2,m}}{\mathrm{d}\eta}\right) \tag{A14}$$

In above (A11), (A13) and (A14), the derivatives of $\chi_{i,m}$ and $\xi_{i,m}$ are non-zero only on the crack-tip element. On the straight-line crack-tip element for pth crack increment, $\chi_{i,m}$ and $\xi_{i,m}$ are expressed as follows:

$$\chi_{i,m} = \delta_{im}\frac{(X^c_i)_p - \chi_i}{l^c_p} \tag{A15}$$

$$\xi_{i,m} = \delta_{im}\frac{(X^c_i)_p - \xi_i}{l^c_p} \tag{A16}$$

DOI: 10.1002/nme

A.3. Derivatives of L and with respect to crack-tip position

The derivatives of L and α are derived by the direct differentiation of (20) and (26), respectively, as follows:

$$\frac{\partial L}{\partial \hat{X}_1^c} = \frac{\hat{X}_1^c}{2\hat{X}_2^c}\left(\ln\left|2\hat{X}_2^c + \sqrt{(\hat{X}_1^c)^2 + 4(\hat{X}_2^c)^2}\right| - \ln|\hat{X}_1^c|\right) \tag{A17a}$$

$$\frac{\partial L}{\partial \hat{X}_2^c} = \frac{\sqrt{(\hat{X}_1^c)^2 + 4(\hat{X}_2^c)^2}}{2\hat{X}_2^c} - \frac{(\hat{X}_1^c)^2}{4(\hat{X}_2^c)^2}\left(\ln\left|2\hat{X}_2^c + \sqrt{(\hat{X}_1^c)^2 + 4(\hat{X}_2^c)^2}\right| - \ln|\hat{X}_1^c|\right) \tag{A17b}$$

$$\frac{\partial \alpha}{\partial \hat{X}_1^c} = -\frac{2\hat{X}_2^c}{(\hat{X}_1^c)^2 + 4(\hat{X}_2^c)^2} + \frac{\hat{X}_2^c}{(\hat{X}_1^c)^2 + (\hat{X}_2^c)^2} \tag{A18a}$$

$$\frac{\partial \alpha}{\partial \hat{X}_2^c} = \frac{2\hat{X}_1^c}{(\hat{X}_1^c)^2 + 4(\hat{X}_2^c)^2} - \frac{\hat{X}_1^c}{(\hat{X}_1^c)^2 + (\hat{X}_2^c)^2} \tag{A18b}$$

A.4. Derivatives of K_{eq}^R and φ with respect to SIFs

The derivatives of K_{eq}^R and φ with respect to SIFs are obtained by the direct differentiation of (8) and (10), respectively, as follows:

$$\frac{\partial K_{\mathrm{eq}}}{\partial \mathbf{K}} = \left(\frac{\partial K_{\mathrm{eq}}}{\partial K_{\mathrm{II}}}, \frac{\partial K_{\mathrm{eq}}}{\partial K_{\mathrm{I}}}\right) = \left(-3\cos^2\frac{\varphi}{2}\sin\frac{\varphi}{2}, \cos^3\frac{\varphi}{2}\right) \tag{A19}$$

$$\frac{\partial \varphi}{\partial \mathbf{K}} = \left(\frac{\partial \varphi}{\partial K_{\mathrm{II}}}, \frac{\partial \varphi}{\partial K_{\mathrm{I}}}\right) = -\frac{1}{K_{\mathrm{I}}\cos\varphi - 3K_{\mathrm{II}}\sin\varphi}(3\cos\varphi - 1, \sin\varphi) \tag{A20}$$

ACKNOWLEDGEMENTS

This work is a part of a research project supported by the Korea Ministry of Construction & Transportation through the Korea Bridge Design & Engineering Research Center at Seoul National University. The authors wish to express their gratitude for the financial support.

REFERENCES

1. Bannantine JA, Comer JJ, Handrock JL. *Fundamentals of Metal Fatigue Analysis*. Prentice-Hall: Englewood Cliffs, NJ, 1990.
2. Barsom JM, Rolfe ST. *Fracture and Fatigue Control in Structures*: *Applications of Fracture Mechanics* (3rd edn). Butterworth-Heinemann: Philadelphia, 1999.
3. Qian J, Fatemi A. Mixed mode fatigue crack growth: a literature survey. *Engineering Fracture Mechanics* 1996; **55**:969–990.
4. Besterfield GH, Liu WK, Lawrence MA, Belytschko T. Fatigue crack growth reliability by probabilistic finite elements. *Computer Methods in Applied Mechanics and Engineering* 1991; **86**:297–320.
5. Reimers P. Simulation of mixed mode fatigue crack growth. *Computers and Structures* 1991; **40**(2):339–346.

DOI: 10.1002/nme

6. Lua YJ, Liu WK, Belytschko T. Elastic interactions of a fatigue crack with a micro-defect by the mixed boundary integral method. *International Journal for Numerical Methods in Engineering* 1993; **36**:2743–2759.
7. Kebir H, Roelandt JM, Foulquier J. A new singular boundary element for crack problems: application to bolted joints. *Engineering Fracture Mechanics* 1999; **62**:497–510.
8. Dell'Erba DN, Aliabadi MH. Three-dimensional thermo-mechanical fatigue crack growth using BEM. *International Journal of Fatigue* 2000; **22**:261–273.
9. Duflot M, Nguyen-Dang H. A meshless method with enriched weight functions for fatigue crack growth. *International Journal for Numerical Methods in Engineering* 2004; **59**:1945–1961.
10. Portela A, Aliabadi MH, Rooke DP. Dual boundary element incremental analysis of crack propagation. *Computers and Structures* 1993; **46**(2):237–247.
11. Mogilevskaya SG. Numerical modeling of 2-D smooth crack growth. *International Journal of Fracture* 1997; **87**:389–405.
12. Stone TJ, Babuška I. A numerical method with a posteriori error estimation for determining the path taken by a propagating crack. *Computer Methods in Applied Mechanics and Engineering* 1998; **160**:245–271.
13. Nishioka T, Tokudome H, Kinoshita M. Dynamic fracture-path prediction in impact fracture phenomena using moving finite element method based on Delaunay automatic mesh generation. *International Journal of Solids and Structures* 2001; **38**:5273–5301.
14. Hong HK, Chen JT. Derivations of integral equations of elasticity. *Journal of Engineering Mechanics* (ASCE) 1988; **114**(6):1028–1044.
15. Portela A, Aliabadi MH, Rooke DP. The dual boundary element method: effective implementation for crack problems. *International Journal for Numerical Methods in Engineering* 1992; **33**:1269–1287.
16. Becker AA. *The Boundary Element Method in Engineering*: *A Complete Course*. McGraw-Hill: London, 1992.
17. Banerjee PK. *The Boundary Element Methods in Engineering* (2nd edn). McGraw-Hill: London, 1994.
18. Gdoutos EE. Fracture mechanics criteria and applications. *Engineering Application of Fracture Mechanics*, vol. 10. Kluwer Academic Publishers: Dordrecht, 1990.
19. Cotterell B, Rice JR. Slightly curved or kinked cracks. *International Journal of Fracture* 1980; **16**(2):155–169.
20. Tai K, Fenner RT. Optimum shape design and positioning of features using the boundary integral equation method. *International Journal for Numerical Methods in Engineering* 1996; **39**:1985–2003.

DOI: 10.1002/nme